American Journal of Ophthalmology Case Reports 36 (2024) 102228

Contents lists available at ScienceDirect

American Journal of Ophthalmology Case Reports

journal homepage: www.ajocasereports.com/

Posterior segment findings in a patient with a *CDHR1* biallelic pathogenic variant

Yusuf Kemal Durlu [a,1,*], Sezin Canbek [b]

[a] Department of Ophthalmology, Makula Eye Health, Istanbul, Turkey
[b] Genomic Laboratory, Umraniye Training and Research Hospital, University of Health Sciences, Istanbul, Turkey

ARTICLE INFO

Keywords:
Cadherin
CDHR1
Optical coherence tomography (OCT)
Retinitis pigmentosa
Major depressive disorder
Non-cystic petaloid maculopathy

ABSTRACT

Purpose: To report the posterior segment findings in a case with a biallelic *CDHR1* frameshift pathogenic variant at chromosome 10 c.616del exon7 p.(His206Thrfs*61).

Observations: A 25-year-old man was diagnosed with retinitis pigmentosa (RP). Fundus examination disclosed bone spicule pigmentation, arteriolar attenuation, peripheral/midperipheral retinal atrophy, and scattered retinal pigment epithelial atrophy/mottling. The wavy appearance of the protrusions located at the inner retinal surface was dispersed from the macula to the midperipheral/peripheral retina in a distinct uniform pattern as observed on structural optical coherence tomography (OCT) images and en-face OCT; the protrusions led to non-cystic petaloid maculopathy. In addition, numerous hyperreflective dots were noticed at the inner limiting membrane level of the temporal macular region. Structural OCT disclosed an increase in choroidal thickness. OCT angiography showed normal retinal vessel density at the superior vascular complex, whereas the deep vascular complex showed a significant reduction in retinal vessel density. The microperimetry showed an abnormal average threshold and abnormal macular integrity, whereas the stability of fixation was completely fulfilled. Photopic/scotopic and multifocal electroretinography findings disclosed subnormal recordings. Psychiatric consultation revealed major depressive disease requiring hospitalization.

Conclusions and importance: Posterior segment findings of RP rather than macular dystrophy were observed in our patient. Inner retinal surface remodeling leading to non-cystic petaloid maculopathy and distinct uniform wavy protrusions extending to the midperipheral/peripheral retinal regions might reveal the involvement of Müller cells in our patient with cadherinopathy. A syndromic association may exist in our patient with a *CDHR1* frameshift pathogenic variant and major depressive disease.

1. Introduction

Cadherins are a member of the calcium-dependent plasma membrane adhesion molecule superfamily responsible for the adherens junctions of the outer blood-retinal barrier, photoreceptor cell maintenance, survival, morphogenesis, and outer segment organization enabling neural circuit formation in the retina.[1–5]

Retinal cadherinopathies are monogenic disorders involving cadherin-related family member 1 (*CDHR1*), *CDH23*, *PCDH15*, and *CDH3* genes.[4] *CDHR1*, previously known as Protocadherin-21 (*PCDH21*), was identified as a candidate gene causing inherited retinal degeneration (IRD).[1,2] Biallelic pathogenic variants in *CDHR1* can develop variable phenotypes of IRD-like cone-rod dystrophy (CORD), rod-cone dystrophy (retinitis pigmentosa [RP]), and late-onset macular dystrophy (LOMD).[2,4] In this case study, the clinical posterior segment findings, including multiple imaging modalities, are reported for a 25-year-old man with the *CDHR1* frameshift pathogenic variant at chromosome 10 c.616del exon7 p.(His206Thrfs*61) leading to typical RP.

After conducting a literature review on September 14, 2024, on PubMed and Google Scholar, and using the keywords, non-cystic petaloid maculopathy and/or non-cystoid petaloid maculopathy, we did not find any previous reports of this en-face optical coherence tomography (OCT) finding.

* Corresponding author.
E-mail address: makulagoz@gmail.com (Y.K. Durlu).
[1] Present address: Dünyagöz Tıp Merkezi, Kazım Özalp Sokak No:25A, Suadiye, Kadıköy, Istanbul 34740, Türkiye.

https://doi.org/10.1016/j.ajoc.2024.102228
Received 26 April 2024; Received in revised form 9 November 2024; Accepted 20 November 2024
Available online 28 November 2024

2. Case report

A 25-year-old man first noted photoaversion and difficulties with dark adaptation and peripheral vision 4 years ago. He had no previous remarkable systemic or ophthalmic history except for a major depressive disorder, which was being treated with sertraline and aripiprazole during hospitalization. The c.616del, p.(His206Thrfs*61) frameshift pathogenic variant was detected as homozygous in our patient's *CDHR1* gene NM_033100.4 transcript. His paternal and maternal grandfathers were first cousins. The CDHR1 pathogenic variant led to an autosomal recessive pattern of inheritance in our patient. The American College of Medical Genetics and Genomics-American Association of Molecular Pathology guidelines were used for the classification of variants.[6] A customized exome panel consisting of 129 known and potential candidate genes was used for the genetic analysis of the patient. Heterozygous pathogenic variants in genes that cause recessive disease were verified by segregation analysis. The pathogenic classification was supported by in silico prediction. We used variant co-occurrence (phasing) information in the gnomAD browser (https://gnomad.broadinstitute.org/variant-cooccurrence) to evaluate whether a pair of variants in a gene occurred in cis (same copy of the gene) or in trans (different copies of the gene). An Illumina NextSeq 500 instrument and the Sophia analysis program were used to interpret the results. The pathogenic variant has not been seen in the 1000G and ESP5400 projects, and validation of the genetic results was performed by next-generation sequencing analysis. The testing laboratory was not CLIA (Clinical Laboratory Improvement Amendments) certified. The patient's best corrected visual acuity was 20/32 in the right eye (OD) and 20/25 in the left eye (OS). The results of an Ishihara pseudo-isochromatic plate color test were normal. Multiple vitreous opacities were seen bilaterally during biomicroscopy. Tonometry recordings were within the normal range.

Fundus and autofluorescence imaging was performed by ultra-wide-field fundus photography (Optos California, Dunfermline, UK). Fig. 1A and B shows peripheral/midperipheral retinal atrophy, bone spicule pigmentation, and scattered retinal pigment epithelial atrophy/mottling in both eyes of our patient. The foveal reflex was pronounced with perifoveolar retinal pigment epithelium (RPE) alterations. The retinal arterioles were mildly attenuated. Surface wrinkling was noticed at the posterior pole of the retina. The optic discs appeared pink with minor temporal chorioretinal atrophy at their temporal margins. Paramacular ring-like hyperautofluorescence and perifoveal/midperipheral mottled hypoautofluorescence were seen during fundus autofluorescence (FAF) imaging (Fig. 1C and D). We observed hypoautofluorescent plaques of various sizes (half to two optic disc diameters) at the temporal peripheral retinal regions in both eyes (Fig. 1C and D).

OCT (Solix; Optovue, Inc., Fremont, CA) recordings revealed severe retinal/macular thinning, sparing the foveal region (Fig. 2A). The central foveal thickness (CFT) was 253 μm in the right eye, and 248 μm in the left eye, respectively. OCT images of the foveal region showed relative structural preservation, and the outer nuclear layer (ONL) and ellipsoid zone (EZ) were clearly delineated at the fovea. However, there was complete loss of the ONL and EZ beginning at the perifoveal region nearly 1500 μm from the center of the foveola (umbo) (Fig. 2B). The retinal layers were disorganized. The macula/retina-vitreous interface was irregular. Several intermittent protrusions were seen at the vitreal surface of the macula/retina. The height of the protrusions varied between 10 and 50 μm. The distance between each apex of the protrusions varied between 70 and 100 μm. The peri-/parafoveal protrusions contributed to the appearance of non-cystic petaloid maculopathy. Atrophy of the RPE was more remarkable at the perifoveal, midperipheral, and peripheral regions, sparing the parafoveal region. Multiple hyperreflective structures were noted between the outer retina and the RPE

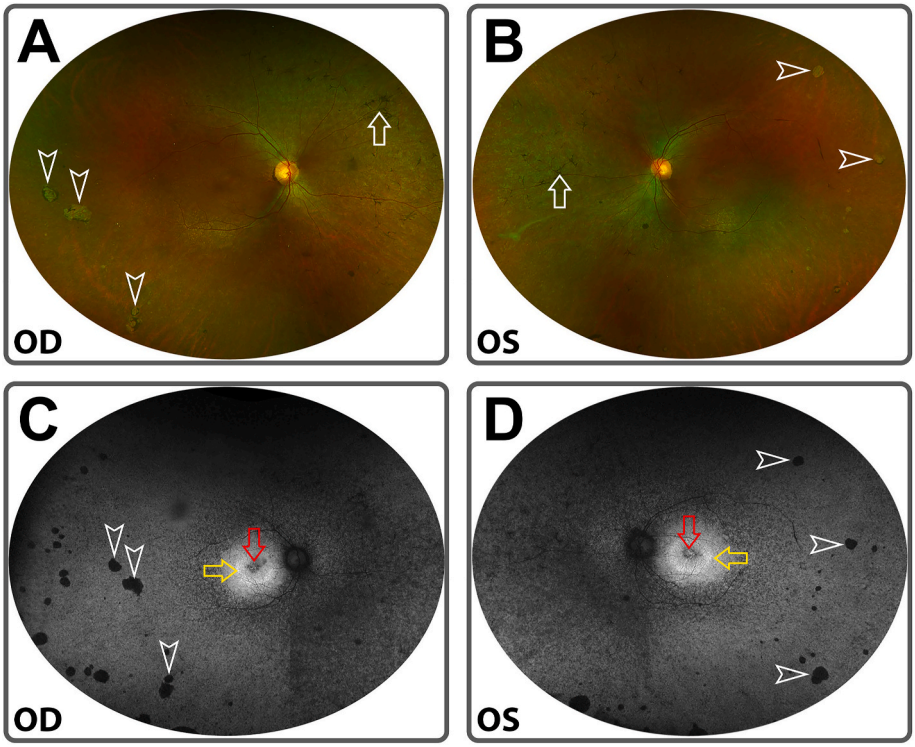

Fig. 1. Ultra-wide-field optomap color images of the right eye (OD) (A) and left eye (OS) (B) show peripheral/midperipheral retinal atrophy, bone spicule pigmentation (white arrow), and scattered retinal pigment epithelial (RPE) atrophy/mottling. The foveal reflex was pronounced with perifoveolar RPE alterations. Shiny reflectance is seen in the peripheral retina. The retinal vessels are mildly attenuated. Patchy retinochoroidal atrophic areas (white arrowhead) are seen predominantly at the temporal peripheral retina. Perifoveal hypoautofluorescence (red arrow), paramacular hyperautofluorescence (yellow arrow), and peripheral patchy hypoautofluorescence plaques (white arrowhead) are noted during autofluorescence imaging of both eyes (C and D). (For interpretation of the references to color in this figure legend, the reader is referred to the Web version of this article.)

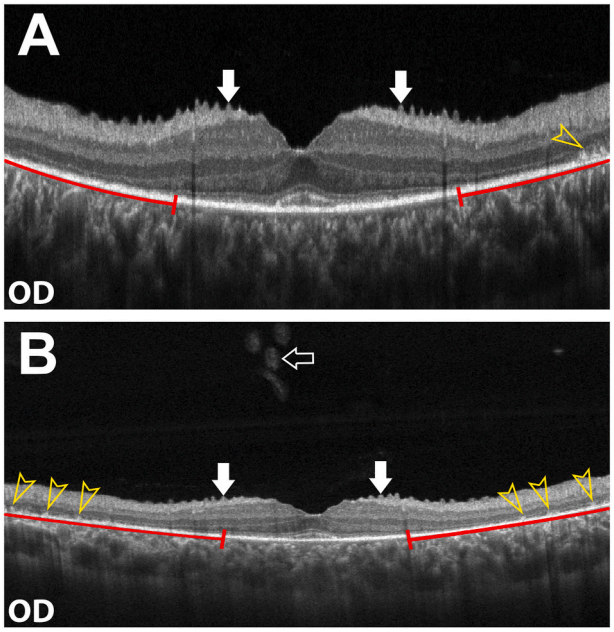

Fig. 2. Spectral-domain optical coherence tomography (SD-OCT) recordings from the right eye show complete loss of the outer nuclear layer (ONL) and ellipsoid zone (EZ) beginning at the perifoveal region nearly 1500 μm from the center of the foveola (umbo) (A, 6-mm OCT scan) and (B, 12-mm OCT scan) (red line). The foveal structures are relatively spared. The ONL and EZ are distinguishable at the fovea (A and B). Intermittent protuberances are observed at the vitreal surface of the macula (white-filled arrow) (A). Several oval hyperreflective structures (white arrow) in the vitreous cavity are observed (B). Multiple hyperreflective structures are noted between the outer retina and the RPE layers (B) (yellow arrowhead). (For interpretation of the references to color in this figure legend, the reader is referred to the Web version of this article.)

layers. Many oval hyperreflective lesions in the vitreous cavity were also seen (Fig. 2B). The choroidal thicknesses were 364 μm in the right eye and 295 μm in the left eye, respectively. The thicknesses of the retinal nerve fiber of the optic nerve heads were 116 μm in the right eye and 122 μm in the left eye, respectively (not shown).

The en-face OCT (3, 6, 9, 12 mm) images revealed a wavy appearance caused by the protrusions at the inner retinal surface (Fig. 3A–H). The wavy pattern extended through the midperipheral/peripheral retina uniformly and was more remarkable on en-face wide-field (9 and 12 mm) OCT recordings (Fig. 3E–H). Numerous hyperreflective dots were noted at the inner limiting membrane level, which were intensified at the macular and midperipheral retinal region temporally (Fig. 3).

OCT angiography (OCTA) revealed that the retinal superficial vascular complex (SVC) was normal (Fig. 4A), whereas the intermediate capillary plexus (ICP) and the deep capillary plexus (DCP), forming the retinal deep vascular complex (DVC), showed a significant reduction in retinal vessel density at the perifoveal region (Fig. 4B). However, relatively normal results were found in the DVC slab at the parafoveal region although the area of the foveal avascular zone was reduced (Fig. 4C). There was no abnormal hypersignal at the outer retina (not shown). The choriocapillaris (CC) slab disclosed hyposignaling and low vessel density at the perifoveal region (Fig. 4D).

The visual field examination revealed generalized visual field constriction leaving the central island (not shown). The results of macular integrity assessment of the microperimetry (MAIA; CenterVue Spa, Padova, Italy) using the 10-2 grid and 4-2 testing strategy showed abnormal average thresholds of 16.7 dB in the right eye (Fig. 5A) and 17.4 dB in the left eye, respectively (Fig. 5B). The standard central (grid 6) microperimetry stimulus pattern includes 37 test locations and the numbers shown represent visual sensitivity in decibels. We found abnormal macular integrity; however, the stability of fixation in our

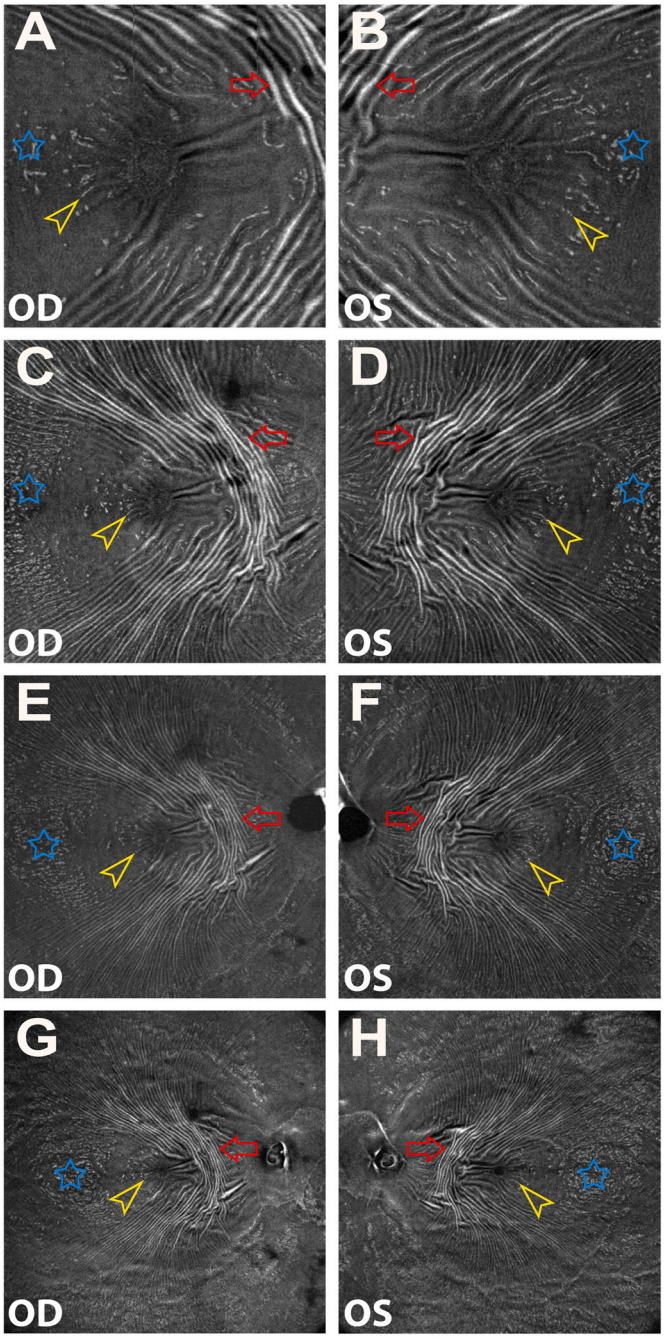

Fig. 3. En face optical coherence tomography (OCT) (derived from 3-, 6-, 9-, and 12-mm scans from top to bottom) images reveal the wavy appearance of the protrusions (red arrow) and hyperreflective dots (blue star) located at the inner retinal surface, and a non-cystic petaloid maculopathy (yellow arrowhead) is noted (A–H, the left column presents scans from the right eye, and the right column presents scans from the left eye). The wavy pattern extends through the midperipheral/peripheral retina uniformly, which is more remarkable in the 6-mm and 9-mm en-face OCT recordings, respectively (C–F). Numerous hyperreflective dots are seen at the inner limiting membrane level, which are intensified at the macular and midperipheral retinal region temporally (blue star). (For interpretation of the references to color in this figure legend, the reader is referred to the Web version of this article.)

patient was completely fulfilled in both eyes. Full-field electroretinography (ffERG) recordings were subnormal under both photopic and scotopic conditions (not shown). Multifocal ERG (RETIscan Multifocal ERG; Roland Consult, Brandenburg, Germany) recordings of our patient, compared with those for a normal individual (Fig. 5C), disclosed

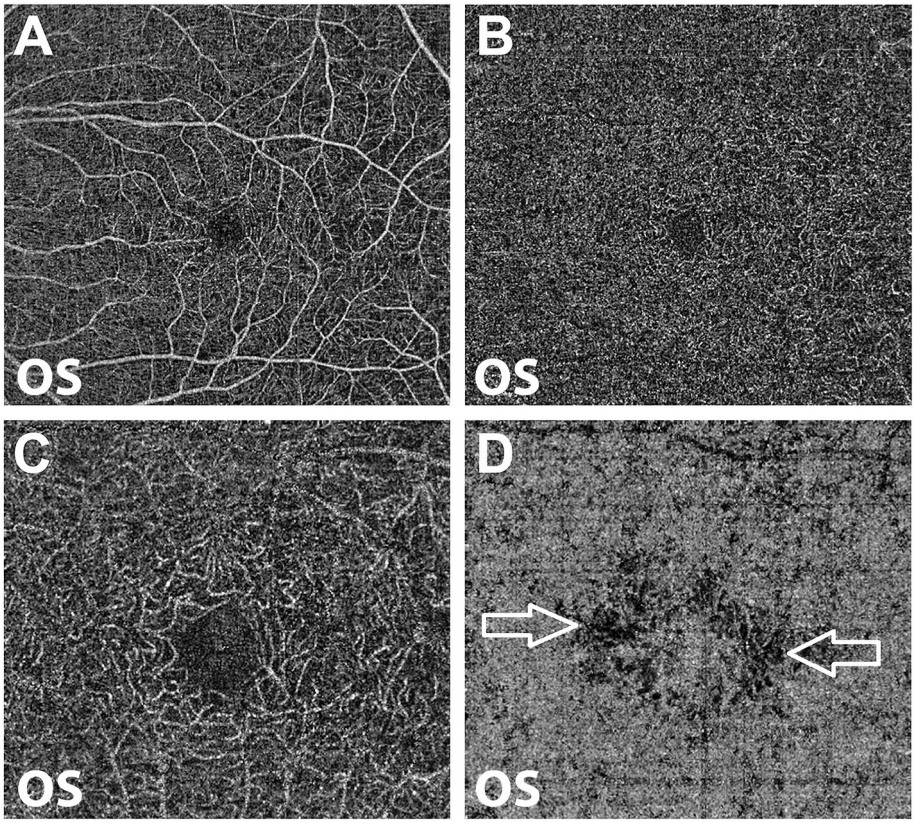

Fig. 4. Optical coherence tomography angiography of the left eye shows that the retinal superficial vascular complex (SVC) is normal (A), whereas the intermediate capillary plexus (ICP) and the deep capillary plexus (DPC), forming the retinal deep vascular complex (DVC), disclose a significant reduction in retinal vessel density at the perifoveal region (B and C). Patchy hyposignaling at the perifoveal region (white arrow) is seen at the choroidal slab (D).

bilateral subnormal results in which the right eye (Fig. 5D) was affected more than the left eye (Fig. 5E), as shown by response density 3D plots derived from the trace array data.

3. Discussion

CDHR1, a photoreceptor-specific member of the cadherin superfamily, has been reported as a candidate gene for IRD.[1] *CDHR1* is mainly expressed at the base of the outer segment at the junction between the rod/cone photoreceptor outer segments.[4,5] Biallelic truncating pathogenic variants in *CDHR1* are characterized by progressive retinal ONL thinning, leading to CORD, RP, and LOMD.[1–4] The phenotype of patients with cadherinopathy shows clinical diversity with respect to disease onset and primary insult.[3,7–15] Here, we report the functional and structural observations for 1 bp deletion in the *CDHR1* gene, resulting in a frameshift and premature termination codon. Two unrelated pathogenic reports on the same 10q23.1 cytogenetic location in the *CDHR1* variant, named NM_033100.4: c.616del (p.His206fs), are cited in the ClinVar database as causing cone-rod dystrophy 15 disease (CORD15); however, no functional evidence is reported in ClinVar (https://www.ncbi.nlm.nih.gov/clinvar/variation/931851/). This sequence change creates a premature translational stop signal (p.His206Thrfs*61) in the *CDHR1* gene. The variation in the transcript is predicted to be degraded by the nonsense-mediated decay mechanism. It is likely to be a null allele (complete loss of protein or complete loss of function). A *CDHR1* pathogenic variant (nonsense, frameshift, splice site ±1, 2) may lead to RNA degradation, thus inhibiting protein formation and/or function. In silico tools indicate that the pathogenic variant may have a disruptive effect on the protein.

RP, macular dystrophy, and CORD15 caused by *CDHR1* pathogenic variants lead to an autosomal recessive pattern of inheritance as reported in ClinVar.[7–15] In our patient with the *CDHR1* pathogenic variant (c.616del (p.His206fs)), we found clinical signs of the RP phenotype (or rod-cone dystrophy); the main retinal findings included generalized retinal atrophy, arteriolar attenuation, bone spicule pigmentation, and scattered RPE mottling. The finding of paramacular ring-like hyperautofluorescence on FAF imaging might have been caused by abnormal accumulation of lipofuscin in the RPE as a result of IRD progression.[9] We also noted areas of perifoveal and midperipheral hypoautofluorescence, indicating RPE atrophy. In the peripheral retina, FAF images revealed discrete patchy areas of hypoautofluorescence in our patient. There have been several reports on patients with IRDs, including *CDHR1*-related retinopathy, showing FAF images with a hyperautofluorescent ring surrounding a central retina of speckled hypoautofluorescence.[10,11]

The phenotype and genotype characteristics of *CDHR1* pathogenic variants show wide clinical heterogeneity and variable expressivity leading to RP, LOMD, and CORD15.[3,4,7–15] A clinical study of patients with novel *CDHR1* genotypes associated with LOMD identified new genotypes for predominantly macular disease in *CDHR1*-associated retinopathy, whereas an association between the p.[Pro261 =] pathogenic variant and macular dystrophy was unveiled.[8,13] There are two separate case reports on the autosomal recessive pattern of inheritance: one is about CORD patients caused by a *PCDH21(CDHR1)* frameshift pathogenic variant, and the other is about CORD 15 caused by a *CDHR1* (c.783G > A) pathogenic variant.[14,15] OCT revealed extensive ONL thinning and EZ pathology at the perifoveal, midperipheral, and peripheral retina, whereas the foveal structures were relatively preserved with normal CFT in our patient, who had relatively preserved central visual acuity measurements, normal color discrimination by Ishihara test, and excellent fixation stability recorded by microperimetry. However, the low average threshold and abnormal macular integrity found

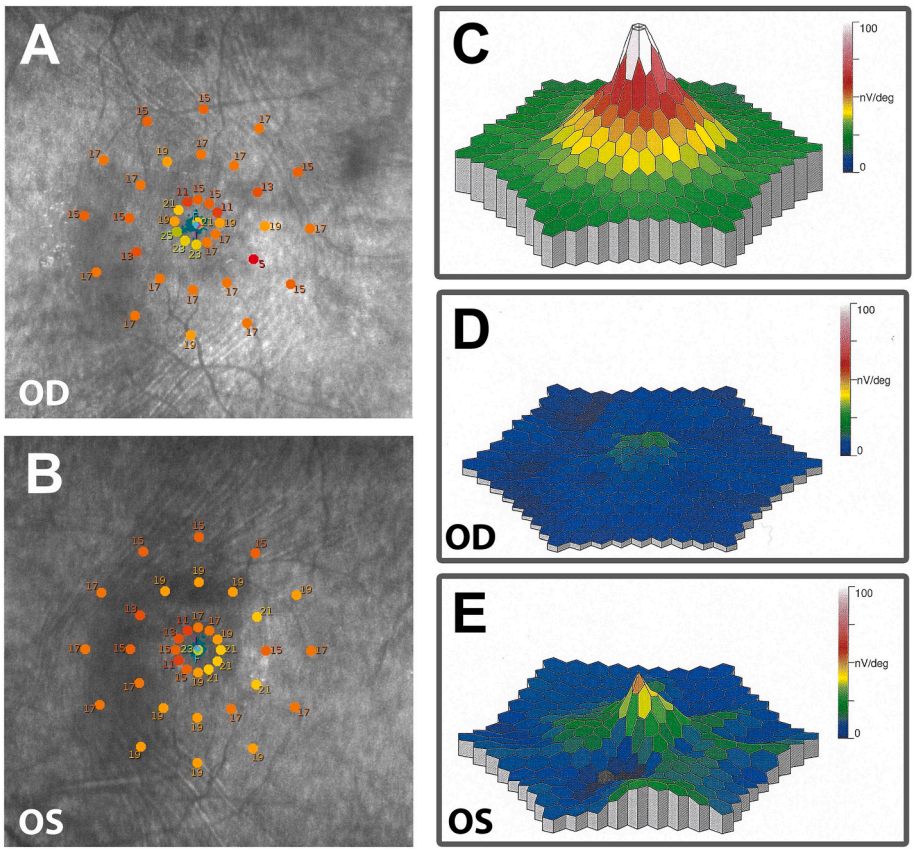

Fig. 5. The standard central (grid 6) microperimetry stimulus patterns of both eyes disclose abnormal average thresholds: 16.7 dB (dB) for the right eye (A), and 17.4 dB for the left eye (B). This stimulus pattern includes 37 test locations, and the numbers shown represent visual sensitivity in dB. The stability of fixation is completely fulfilled (blue dots in the central region). Multifocal electroretinography (ERG) recordings are compared with those to a normal individual (C); response density 3D plots were derived from the trace array data. The multifocal ERG results for the right eye (D) disclose a more severe reduction in response density than for the left eye (E). (For interpretation of the references to color in this figure legend, the reader is referred to the Web version of this article.)

by microperimetry together with subnormal multifocal ERG results disclosed a functional macular deficit, which is a common clinical finding in patients with RP progression.

Foveal OCT revealed relatively preserved retinal layers except for the wavy appearance of the inner retinal layer facing the endfoot of Müller cells. The distinct en-face imaging created by the symmetrical protrusions (possibly endfoot of Müller cells) at the inner retinal surface, extending through the midperipheral and peripheral retina in a distinct pattern, and the non-cystic petaloid maculopathy seen on en-face OCT imaging is a novel finding in our patient with cadherinopathy.

There has been no clinical report on the dysfunction of cadherins leading to inner retinal pathology.[4] However, it has been reported that multiple subtypes of cadherins are expressed in the ganglion cell layer (amacrine, bipolar, and horizontal cells) and Müller cells in the retina, including RPE.[16] An experimental CRISPR-based reverse genetic study disclosed that the *CDHR1* gene might have a role in the morphological features of Müller cells, including tiling across the tangential plane.[17] Cadherins are calcium-dependent intercellular adhesion molecules and are considered to be regulators of cell morphogenesis/polarity.[3] The uniform wavy protrusions at the macular and midperipheral/peripheral retina and non-cystic petaloid maculopathy observed by en-face OCT might reflect the inner retinal pathology in our case. The Müller cells might act as living optical fibers or light collectors, which might transfer light with low scattering from the inner retinal surface to the photoreceptors.[18] The morphological re-arrangement of the Müller cells as shown by en-face OCT might enhance the development of photoaversion symptoms in our patient.

Several cottonball/snowball-like and spindle-shaped vitreous opacities were seen in our patient. Takahashi et al. reported that vitreous opacities were found in nine of ten patients with RP.[19] The proinflammatory cytokines and chemokines such as monocyte chemotactic protein-1 were increased in aqueous and vitreous humor, indicating sustained chronic inflammation in the eyes of patients with RP.[20] The relationship between the presence of vitreous opacities and the tendency to inflammation in our patient is in accordance with the previous reports.

We observed hyperreflective dots subretinally during structural OCT. The expression of cadherin in RPE cells might be crucial for the differentiation of epithelial cell phenotypes and planar cell polarity in situ.[16] The hyperreflective lesions seen during OCT might be due to fragmented/disorganized outer segments.[21] We observed subretinal hyperreflective lesions in the rod-dominant midperipheral region but not in the cone-dominant macular region. The *CDHR1* frameshift pathogenic variant might lead to a complete loss of cadherin protein and its function at the RPE cells, which might accelerate severe rod degeneration in our case.

The choroidal thickness was increased in our patient. It has been reported previously that the submacular choroidal thickness was significantly reduced in patients with RP.[22] In patients with cystoid macular edema associated with RP, the subfoveal choroidal thickness was increased with a reduced choroidal vascularity index.[23] The mean age of patients with RP in the previous reports was between the fourth and fifth decades.[22,23] Our patient was 25 years of age and had mild RP, relatively sparing the fovea with normal CFT without cystoid macular edema.

The OCTA results showed that the SVC was normal, whereas the ICP and DCP forming DVC revealed a significant reduction in retinal vessel density at the perifoveal region in our patient. However, normal results

were found in SVC and DVC at the parafoveal region other than a reduction around the foveal avascular zone. Hagag et al. reported that retinal DVC of patients with RP showed a marked reduction in vessel density with relative sparing of the SVC.[24] The OCTA findings in our patient were similar to the OCTA findings in patients with RP.[24] The retinal vascular remodeling in patients with RP and in our patient could be attributed to the loss of photoreceptors, leading to ONL thinning, which might cause a decrease in the metabolism of the outer retinal layers. We also observed that the DVC was relatively spared, which might be correlated with the relative preservation of foveal structure and function in our patient. The OCTA of the CC slab disclosed patchy hyposignaling at the perifoveal region where hypoautofluorescence was seen. This might be related to the CC atrophy observed under RPE atrophy in those areas in our patient because the foveal CC vessel density was reported to be reduced in patients with severe RP.[25]

Our patient was diagnosed with major depressive disorder requiring hospitalization. Cadherins may play a pivotal role in the regulation of neural tube regionalization, neuronal migration, gray matter differentiation, neural circuit/synapse formation, and synaptic remodeling in the central nervous system.[26] Dysfunction of the cadherin-based adhesive system may alter functional connectivity and coherent information processing in neuropsychiatric disorders.[26] *CDHR1* RNA is expressed not only in the retina but also in the cerebral cortex, basal ganglia, pons, and medulla.[4] *CDHR1*, *CDH3*, *PCDH15*, and *CDH23* are known as cadherins encoded by genes associated with monogenic IRD.[4] *CDHR1*, *PCDH15*, and *CDH23* have been implicated in susceptibility to neuropsychiatric disorders.[27–29] However, Hahm et al. reported that patients with RP are at increased risk of depression, which was found to be a unique contributing factor influencing their vision-related quality of life, independent of demographic status, objective visual function, and severity of ocular disease severity.[30] Correlation between the coexistence of RP caused by biallelic *CDHR1* pathogenic variants and neuropsychiatric disorders remains to be explored.

4. Conclusions

Our patient with the *CDHR1* frameshift pathogenic variant disclosed posterior segment findings of RP with peripheral/midperipheral retinal atrophy, bone spicule pigmentation, and scattered RPE atrophy/mottling whereas the foveal functions were relatively preserved. Remodeling of the inner retinal layers characterized by uniform wavy protrusions and non-cystic petaloid maculopathy as shown by en-face and structural OCT might reveal the involvement of Müller cells, leading to inner retinal pathology in our patient with cadherinopathy.

CRediT authorship contribution statement

Yusuf Kemal Durlu: Writing – review & editing, Writing – original draft, Visualization, Validation, Funding acquisition, Conceptualization. **Sezin Canbek:** Validation, Methodology.

Patient consent

Written and signed informed consent was given by the patient to publish his case report including the publication of images. The study adhered to the tenets of the Declaration of Helsinki. This study protocol was reviewed, and the need for approval was waived by the Bahçeşehir University School of Medicine Ethical Committee (approved on April 9, 2021), Istanbul.

Funding

The publication was supported in part by Makula Eye Health, Inc., Istanbul, Turkey.

Declaration of competing interest

The authors declare the following financial interests/personal relationships which may be considered as potential competing interests: The authors have no conflict of interest.

Acknowledgment

The authors acknowledge Professor Elias Traboulsi for valuable suggestions during the preparation of the manuscript. The authors are also grateful to Lorna O'Brien for help with language correction.

Abbreviations

CC, choriocapillaris; CFT, central foveal thickness; CORD, cone-rod dystrophy; DCP, deep capillary plexus; DVC, deep vascular complex; ERG, electroretinography; EZ, ellipsoid zone; FAF, fundus autofluorescence; ffERG, full-field electroretinography; ICP, intermediate capillary plexus; IRD, inherited retinal degeneration; LOMD, late-onset macular dystrophy; OCT, optical coherence tomography; OCTA, optical coherence tomography angiography; OD, right eye; ONL, outer nuclear layer; OS, left eye; RP, retinitis pigmentosa; RPE, retinal pigment epithelium; SD-OCT, spectral-domain optical coherence tomography (SD-OCT); SVC, superficial vascular complex.

References

1. Bolz H, Ebermann I, Gal A. Protocadherin-21 (PCDH21), a candidate gene for human retinal dystrophies. *Mol Vis*. 2005;11:929–933.
2. Henderson RH, Li Z, Abd El Aziz MM, et al. Biallelic mutation of protocadherin-21 (PCDH21) causes retinal degeneration in humans. *Mol Vis*. 2010;16:46–52.
3. Stingl K, Mayer AK, Llavona P, et al. CDHR1 mutations in retinal dystrophies. *Sci Rep*. 2017;7(1):6992. https://doi.org/10.1038/s41598-017-07117-8.
4. Yusuf IH, Garrett AM, MacLaren RE, Charbel Issa P. Retinal cadherins and the retinal cadherinopathies: current concepts and future directions. *Prog Retin Eye Res*. 2022; 90, 101038. https://doi.org/10.1016/j.preteyeres.2021.101038.
5. Rattner A, Smallwood PM, Williams J, et al. A photoreceptor-specific cadherin is essential for the structural integrity of the outer segment and for photoreceptor survival. *Neuron*. 2001;32(5):775–786. https://doi.org/10.1016/S0896-6273(01)00531-1.
6. Richards S, Aziz N, Bale S, et al. Standards and guidelines for the interpretation of sequence variants: a joint consensus recommendation of the American College of Medical genetics and Genomics and the association for molecular pathology. *Genet Med*. 2015;17(5):405–424. https://doi.org/10.1038/gim.2015.30.
7. Cohen B, Chervinsky E, Jabaly-Habib H, Shalev SA, Briscoe D, Ben-Yosef T. A novel splice site mutation of CDHR1 in a consanguineous Israeli Christian Arab family segregating autosomal recessive cone-rod dystrophy. *Mol Vis*. 2012;18:2915–2921.
8. Ba-Abbad R, Sergouniotis PI, Plagnol V, et al. Clinical characteristics of early retinal disease due to CDHR1 mutation. *Mol Vis*. 2013;19:2250–2259.
9. Robson AG, El-Amir A, Bailey C, et al. Pattern ERG correlates of abnormal fundus autofluorescence in patients with retinitis pigmentosa and normal visual acuity. *Invest Ophthalmol Vis Sci*. 2003;44(8):3544. https://doi.org/10.1167/iovs.02-1278, 3450.
10. Bessette AP, DeBenedictis MJ, Traboulsi EI. Clinical characteristics of recessive retinal degeneration due to mutations in the CDHR1 gene and a review of the literature. *Ophthalmic Genet*. 2018;39(1):51–55. https://doi.org/10.1080/13816810.2017.1363244.
11. Georgiou M, Robson AG, Fujinami K, et al. Phenotyping and genotyping inherited retinal diseases: molecular genetics, clinical and imaging features, and therapeutics of macular dystrophies, cone and cone-rod dystrophies, rod-cone dystrophies, Leber congenital amaurosis, and cone dysfunction syndromes. *Prog Retin Eye Res*. 2024; 100, 101244. https://doi.org/10.1016/j.preteyeres.2024.101244.
12. Dawood M, Lin S, Din TU, et al. Novel mutations in PDE6A and CDHR1 cause retinitis pigmentosa in Pakistani families. *Int J Ophthalmol*. 2021;14(12):1843–1851. https://doi.org/10.18240/ijo.2021.12.06.
13. Malechka VV, Cukras CA, Chew EY, et al. Clinical phenotypes of CDHR1-associated retinal dystrophies. *Genes*. 2022;13(5):925. https://doi.org/10.3390/genes13050925.
14. Ostergaard E, Batbayli M, Duno M, Vilhelmsen K, Rosenberg T. Mutations in PCDH21 cause autosomal recessive cone-rod dystrophy. *J Med Genet*. 2010;47(10):665–669. https://doi.org/10.1136/jmg.2009.069120.
15. Sobolewska M, Świerczyńska M, Dorecka M, Wyględowska-Promieńska D, Krawczyński MR, Mrukwa-Kominek E. CDHR1-related cone-rod dystrophy: clinical characteristics, imaging findings, and genetic test results-a case report. *Medicina (Kaunas)*. 2023;59(2):399. https://doi.org/10.3390/medicina59020399.
16. Honjo M, Tanihara H, Suzuki S, Tanaka T, Honda Y, Takeichi M. Differential expression of cadherin adhesion receptors in neural retina of the postnatal mouse. *Invest Ophthalmol Vis Sci*. 2000;41(2):546–551.

17. Charlton-Perkins M, Almeida AD, MacDonald RB, Harris WA. Genetic control of cellular morphogenesis in Müller glia. *Glia*. 2019;67(7):1401–1411. https://doi.org/10.1002/glia.23615.
18. Franze K, Grosche J, Skatchkov SN, et al. Muller cells are living optical fibers in the vertebrate retina. *Proc Natl Acad Sci U S A*. 2007;104(20):8287–8292. https://doi.org/10.1073/pnas.0611180104.
19. Takahashi M, Jalkh A, Hoskins J, Trempe CL, Schepens CL. Biomicroscopic evaluation and photography of liquefied vitreous in some vitreoretinal disorders. *Arch Ophthalmol*. 1981;99(9):1555–1559. https://doi.org/10.1001/archopht.1981.03930020429003.
20. Yoshida N, Ikeda Y, Notomi S, et al. Clinical evidence of sustained chronic inflammatory reaction in retinitis pigmentosa. *Ophthalmology*. 2013;120(1):100–105. https://doi.org/10.1016/j.ophtha.2012.07.006.
21. Duncan JL, Roorda A, Navani M, et al. Identification of a novel mutation in the CDHR1 gene in a family with recessive retinal degeneration. *Arch Ophthalmol*. 2012;130(10):1301–1308. https://doi.org/10.1001/archophthalmol.2012.1906.
22. Dhoot DS, Huo S, Yuan A, et al. Evaluation of choroidal thickness in retinitis pigmentosa using enhanced depth imaging optical coherence tomography. *Br J Ophthalmol*. 2013;97(1):66–69. https://doi.org/10.1136/bjophthalmol-2012-301917.
23. Iovino C, Au A, Hilely A, et al. Evaluation of the choroid in eyes with retinitis pigmentosa and cystoid macular edema. *Invest Ophthalmol Vis Sci*. 2019;60(15):5000–5006. https://doi.org/10.1167/iovs.19-27300.
24. Hagag AM, Wang J, Lu K, et al. Projection-resolved optical coherence tomographic angiography of retinal plexuses in retinitis pigmentosa. *Am J Ophthalmol*. 2019;204:70–79. https://doi.org/10.1016/j.ajo.2019.02.034.
25. Ong SS, Liu TYA, Li X, Singh MS. Choriocapillaris flow loss in center-involving retinitis pigmentosa: a quantitative optical coherence tomography angiography study using a novel classification system. *Graefes Arch Clin Exp Ophthalmol*. 2021;259(11):3235–3242. https://doi.org/10.1007/s00417-021-05223-y.
26. Redies C, Hertel N, Hübner CA. Cadherins and neuropsychiatric disorders. *Brain Res*. 2012;1470:130–144. https://doi.org/10.1016/j.brainres.2012.06.020.
27. Zhang T, Hou L, Chen DT, McMahon FJ, Wang JC, Rice JP. Exome sequencing of a large family identifies potential candidate genes contributing risk to bipolar disorder. *Gene*. 2018;645:119–123. https://doi.org/10.1016/j.gene.2017.12.025.
28. Ishizuka K, Kimura H, Wang C, et al. Investigation of rare single-nucleotide PCDH15 variants in schizophrenia and autism spectrum disorders. *PLoS One*. 2016;11(4),e0153224. https://doi.org/10.1371/journal.pone.0153224.
29. Balan S, Ohnishi T, Watanabe A, et al. Role of an atypical cadherin gene, Cdh23 in prepulse inhibition, and implication of CDH23 in schizophrenia. *Schizophr Bull*. 2021;47(4):1190–1200. https://doi.org/10.1093/schbul/sbab007.
30. Hahm BJ, Shin YW, Shim EJ, et al. Depression and the vision-related quality of life in patients with retinitis pigmentosa. *Br J Ophthalmol*. 2008;92(5):650–654. https://doi.org/10.1136/bjo.2007.127092.